

**Figure 9** Analysis of gain enhancement at low-elevation angles (a) amplitude and phase of the induced current and (b) gain enhancement at  $\theta = 75^\circ$

#### 4. CONCLUSION

We investigated the design of a microstrip patch antenna with improved low-elevation gain for CRPA applications. The proposed antenna is composed of the main patch and a subpatch, and the two patches were designed to be electromagnetically coupled for the same direction current by adjusting the size of the subpatch and the substrate height. The proposed antenna was fabricated and mounted on a 140-mm circular ground platform to measure its antenna characteristics. The measured reflection coefficient was  $-11.2$  dB at 1575 MHz with a bore-sight gain of 5.1 dBic, and the average gain at  $\theta = 75^\circ$  was  $-1.7$  dBic with an average HPBW of  $165^\circ$ . The results proved that the proposed antenna is suitable to enhance the low-elevation gain and can be used as the individual element of CRPA arrays.

#### ACKNOWLEDGMENTS

This research was supported by Civil Military Technology Cooperation (CMTC) and the Basic Science Research Program through the National Research Foundation of Korea (NRF) funded by the Ministry of Education (NRF-2014R1A1A2055813).

#### REFERENCES

- J.R. Lambert, C.A. Balanis, and D. DeCarlo, Spherical cap adaptive antennas for GPS, *IEEE Antennas Propag Mag* 57 (2009), 406–413.

- P. Enge, T. Walter, S. Pullen, C. Kee, Y.C. Chao, and Y.J. Tsai, Wide area augmentation of the global positioning system, *IEEE Proc Mag* 84 (1996), 1063–1088.
- S. Datta-Barua, J. Lee, S. Pullen, M. Luo, A. Ene, D. Qiu, G. Zhang, and P. Enge, Ionospheric threat parameterization for local area global-positioning-system-based aircraft landing systems, *J Air* 47 (2010), 1141–1151.
- F.S. Chang, K.L. Wong, and T.W. Chiou, Low-cost broadband circularly polarized patch antenna, *IEEE Antennas Propag Mag* 51 (2003), 3006–3009.
- T.N. Chang and J.M. Lin, Circularly polarized antenna having two linked slot-rings, *IEEE Antennas Propag Mag* 59 (2011), 3057–3060.
- K.L. Wong and Y.F. Lin, Circularly polarised microstrip antenna with a tuning stub, *IEEE Electron Lett* 34 (1998), 831–832.
- H.M. Chen and K.L. Wong, On the circular polarization operation of annular-ring microstrip patch antennas, *IEEE Antennas Propag Mag* 47 (1999), 1289–1292.
- W.S. Chen, C.K. Wu, and K.L. Wong, Single-feed square-ring microstrip antenna with truncated corners for compact circular polarisation operation, *Electron Lett* 34 (1998), 1045–1047.
- G. Byun, S. Kim, and H. Choo, Design of a dual-band GPS antenna using a coupled feeding structure for high isolation in a small array, *Microwave Opt Technol Lett* 56 (2014), 359–361.
- G. Byun, S.M. Seo, I. Park, and H. Choo, Design of small CRPA arrays for dual-band GPS applications, *IEICE Trans Commun E97B* (2014), 1130–1138.
- Y. Rahmat-samii and E. Michielssen, *Electromagnetic optimization by genetic algorithms*, Wiley, New York, 1999.
- FEKO Suite 7.0, EM software and systems, Available at: <http://www.feko.info>, 2014.

© 2016 Wiley Periodicals, Inc.

## 8-ANTENNA AND 16-ANTENNA ARRAYS USING THE QUAD-ANTENNA LINEAR ARRAY AS A BUILDING BLOCK FOR THE 3.5-GHz LTE MIMO OPERATION IN THE SMARTPHONE

Kin-Lu Wong,<sup>1</sup> Jun-Yu Lu,<sup>1</sup> Li-Yu Chen,<sup>1</sup> Wei-Yu Li,<sup>2</sup> and Yong-Ling Ban<sup>3</sup>

<sup>1</sup>Department of Electrical Engineering, National Sun Yat-Sen University, Kaohsiung 80424, Taiwan; Corresponding author: wongkl@ema.ee.nsysu.edu.tw

<sup>2</sup>Information and Communications Research Laboratories, Industrial Technology Research Institute, Hsinchu 31040, Taiwan

<sup>3</sup>Institute of Electromagnetics and School of Electrical Engineering, University of Electronic Science and Technology of China, Chengdu 611731, China

Received 19 May 2015

**ABSTRACT:** Using the quad-antenna linear (QAL) array as a building block, the 8-antenna and 16-antenna arrays for the 3.5-GHz long term evolution multiple-input multiple-output (MIMO) operation in the smartphone are demonstrated. The QAL array has a planar structure of narrow width 3 mm ( $0.035\lambda$ ) and short length 50 mm ( $0.58\lambda$ ), with  $\lambda$  being the wavelength at 3.5 GHz. For the 8-antenna array, two QAL arrays are disposed along two opposite side edges (denoted as Array A) or the same side edge (denoted as Array B) of the system circuit board of the smartphone. The obtained envelope correlation coefficient values of the antennas in Array A and B are shown. The calculated channel capacities for Array A and B applied in an  $8 \times 8$  MIMO system are also analyzed. The 16-antenna array formed by four QAL arrays disposed along two opposite side edges (denoted as Array C) is then studied. For operating in a  $16 \times 16$  MIMO system, the calculated channel capacity of Array C can reach about 66–70 bps/Hz with a 20-dB signal-to-noise ratio. The obtained channel capacity is about 5.7–6.1 times that (11.5 bps/Hz) of the upper limit of an ideal  $2 \times 2$  MIMO system with 100% antenna efficiency for

**Key words:** mobile antennas; multiple-input multiple-output antennas; 8-antenna array; 16-antenna array; quad-antenna linear array; smartphone antennas; slot antennas

### 1. INTRODUCTION

For the  $2 \times 2$  long term evolution (LTE) multiple-input multiple-output (MIMO) mobile communication, two antennas with

acceptable isolation are needed to be embedded in the limited space inside the smartphone [1–5]. It is also noted that for the  $2 \times 2$  LTE MIMO operation, the upper limit of the ergodic channel capacity can reach about 11.5 bps/Hz with a 20-dB signal-to-noise (SNR) ratio [6]. The channel capacity can further be greatly increased by increasing the number of the antennas in the MIMO system [7]. However, owing to the limited space inside the smartphone, it is difficult to embed a large number of LTE antennas operated in the 698–960 MHz and/or 1710–2690 MHz bands for the MIMO operation. Conversely, it has been recently demonstrated that a 10-antenna array [6] operating in the new LTE band of 3400–3800 MHz [8–10] is promising to

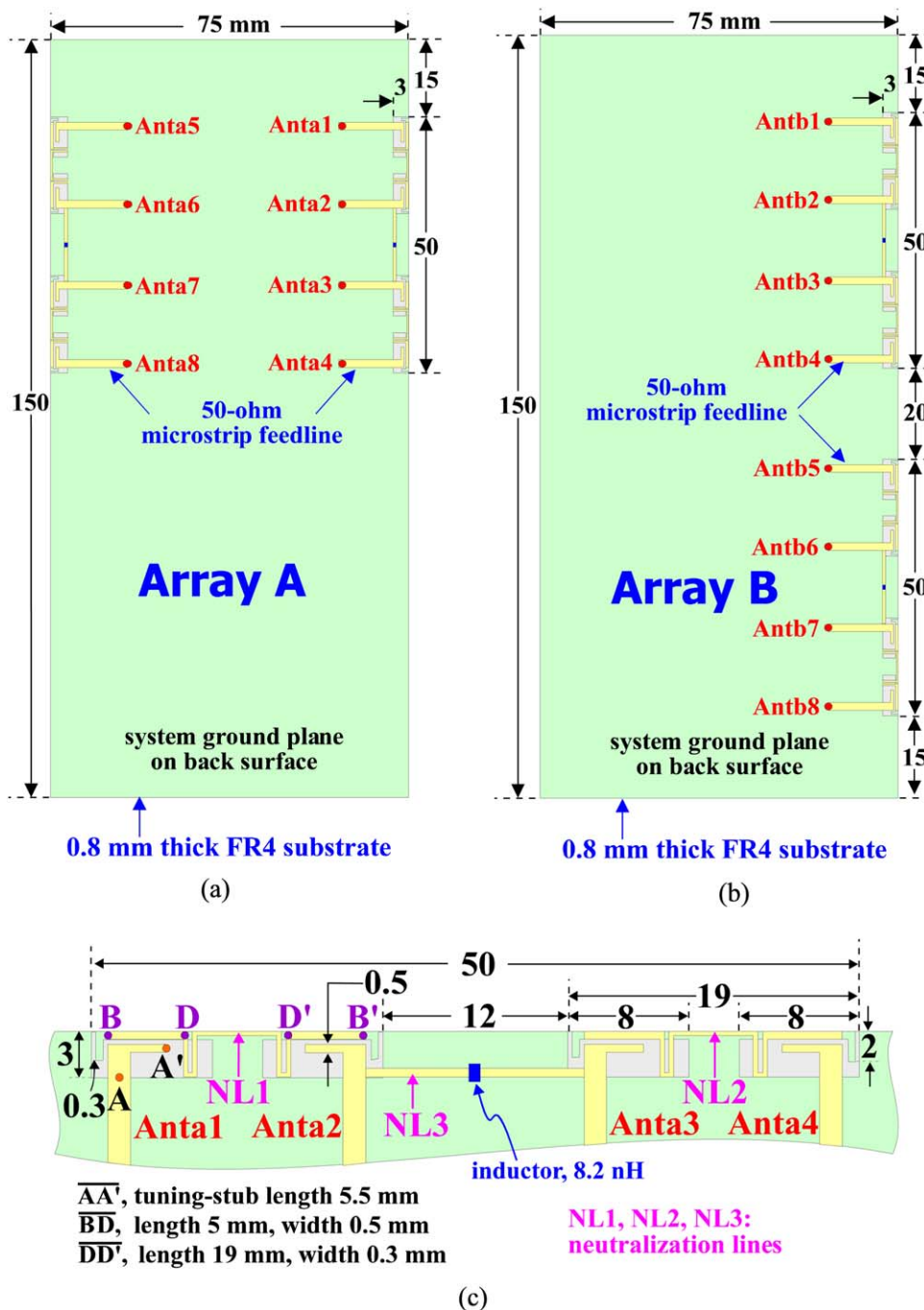


**Figure 1** Geometry of the 8-antenna arrays formed by two QAL arrays. (a) Two QAL arrays disposed along two opposite side edges (Array A), (b) two QAL arrays disposed along the same side edge (Array B) and (c) dimensions of the QAL array comprising Anta1 to Anta4. [Color figure can be viewed in the online issue, which is available at wileyonlinelibrary.com]

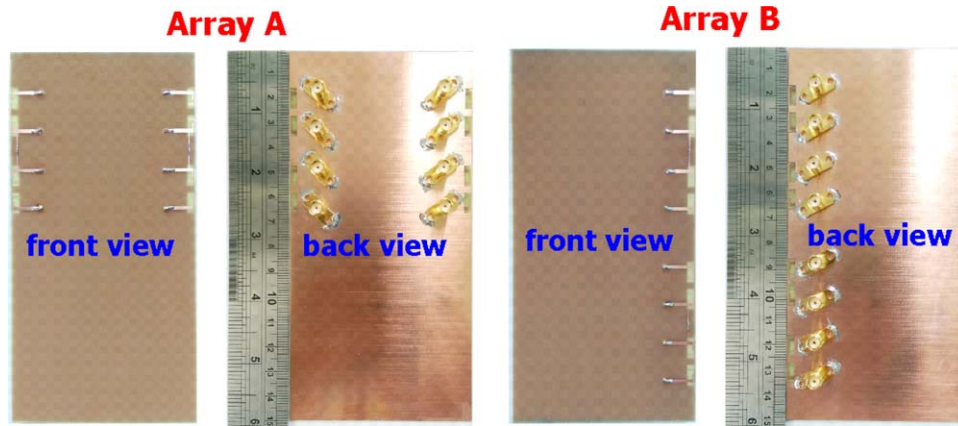


**Figure 2** Photo of the fabricated Array A and B. [Color figure can be viewed in the online issue, which is available at wileyonlinelibrary.com]

be embedded in the smartphone for the  $10 \times 10$  MIMO operation. A maximum channel capacity of about 47 bps/Hz with a 20-dB SNR can be obtained for the 10-antenna array applied in a  $10 \times 10$  MIMO system [6].

In this article, the 8-antenna and 16-antenna arrays obtained using the quad-antenna linear (QAL) array as a building block for the 3.5-GHz (3400–3600 MHz) LTE MIMO operation [8,11] in the smartphone are demonstrated. The QAL array is formed by configuring four decoupled printed slot antennas into a compact linear array, which is promising to be disposed along the narrow region between the display panel and the two long side edges of the smartphone casing. Two cases of the 8-antenna array are studied. The first 8-antenna array is obtained by disposing two QAL arrays disposed along two

opposite side edges of the system circuit board of the smartphone. The second 8-antenna array is achieved by disposing two QAL arrays along the same side edge thereof. For both the 8-antenna arrays, their envelope correlation coefficients (ECCs) [12] obtained from the simulation software HFSS [13] and calculated from the measured complex electric-field patterns of the antennas therein [6] are presented. Their channel capacities for applications in an  $8 \times 8$  MIMO system are also calculated and discussed.

A 16-antenna array obtained by disposing four QAL arrays along two opposite side edges is also studied. The simulated ECC of the antennas in the 16-antenna array and the calculated channel capacity for applications in a  $16 \times 16$  MIMO system are shown. In this study, it is obtained that the peak value of the calculated

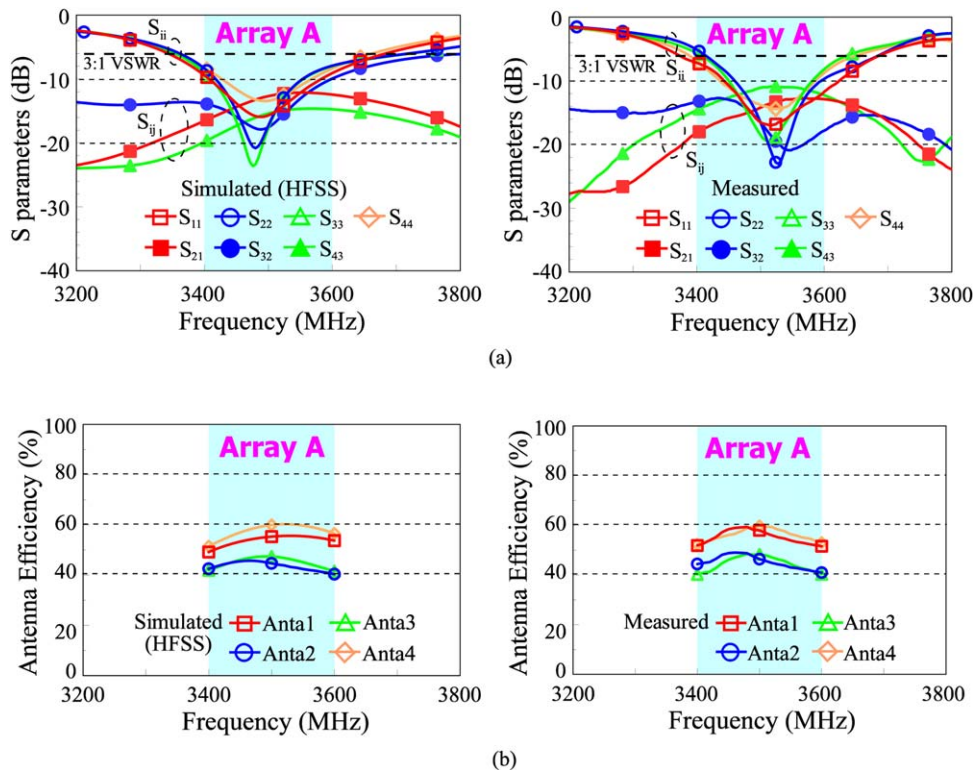


**Figure 3** Measured and simulated (a)  $S$  parameters and (b) antenna efficiencies for four representative antennas (Anta1 to Anta4) in Array A. [Color figure can be viewed in the online issue, which is available at wileyonlinelibrary.com]

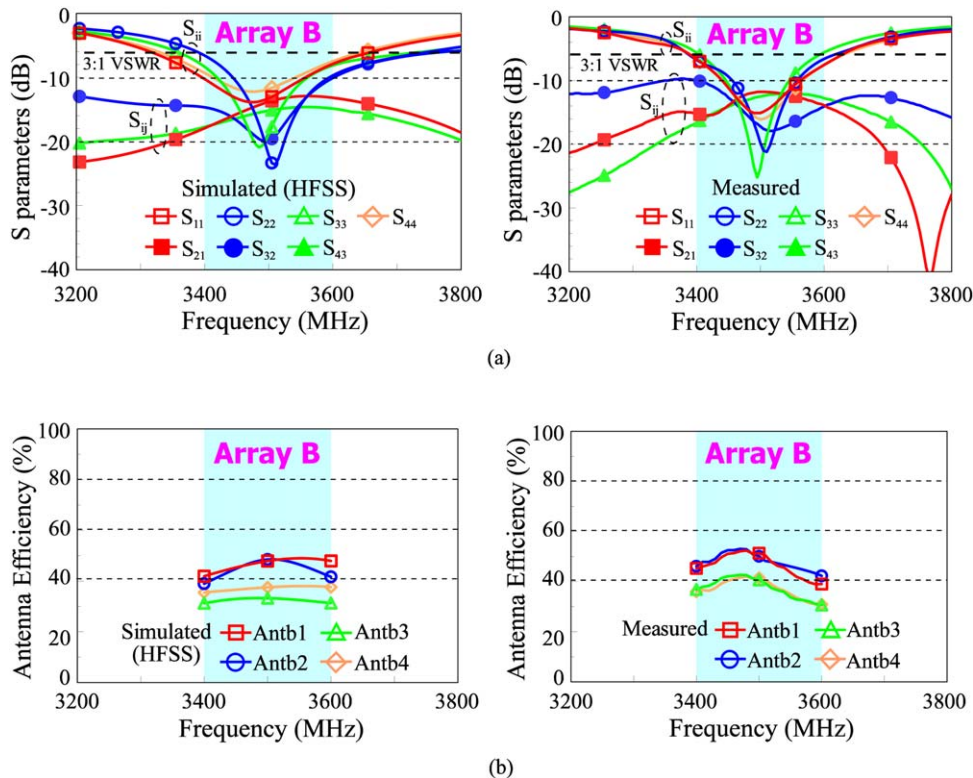


**Figure 4** Measured and simulated (a)  $S$  parameters and (b) antenna efficiencies for four representative antennas (Antb1 to Antb4) in Array B. [Color figure can be viewed in the online issue, which is available at [wileyonlinelibrary.com](http://wileyonlinelibrary.com)]

ergodic channel capacity can reach about 70 bps/Hz with a 20-dB SNR, which is about 6.1 times that (11.5 bps/Hz) of the upper limit of an ideal  $2 \times 2$  MIMO system with 100% antenna efficiency for the transmitting and receiving antennas therein [6].

In this study, the configurations of two 8-antenna arrays and one 16-antenna array obtained using the QAL array as a building block are described, respectively, in Section 2 and 3. Their scattering parameters ( $S_{ij}$ ) and antenna efficiencies of the antennas therein are shown. The obtained ECCs and channel capacities for applications in the  $8 \times 8$  and  $16 \times 16$  MIMO systems are presented and discussed.

## 2. 8-ANTENNA ARRAY

### 2.1. Array Configurations

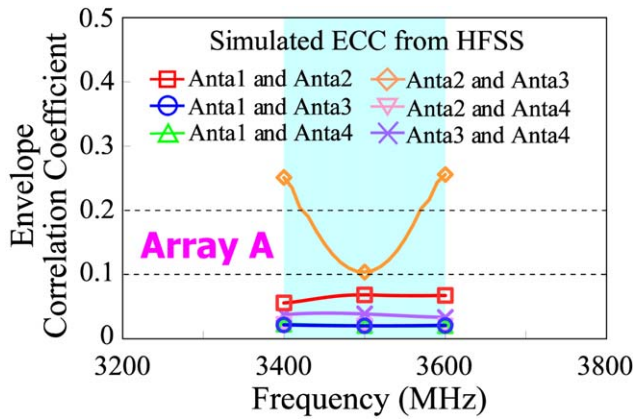
Figure 1 shows the geometry of the 8-antenna arrays formed by two QAL arrays of same dimensions. The first 8-antenna array formed by disposing two QAL arrays along two opposite side edges of the system circuit board of the smartphone is shown in Figure 1(a) and denoted as Array A. The second 8-antenna array shown in Figure 1(b) is formed by disposing two QAL arrays along the same side edge of the system circuit board and is denoted as Array B. Details of the QAL array comprising Anta1 to Anta4 are given in Figure 1(c). Both Array A and B are also fabricated for experimental studies, and their photos are shown in Figure 2 to provide better views of the array configurations. The system circuit board is selected to be a 0.8-mm thick FR4 substrate of width 75 mm and length 150 mm. The selected dimensions of the system circuit board are to simulate the smartphone with a 5.8-inch display panel. Along the top and bottom edges of the system circuit board, it is reserved for accommodating two LTE/WWAN antennas for the 3G/4G opera-

tion, which generally covers the operating bands of 698–960 and 1710–2690 MHz. The two LTE/WWAN antennas are not included in the study. The relative permittivity and loss tangent of the FR4 substrate are 4.4 and 0.02, respectively.

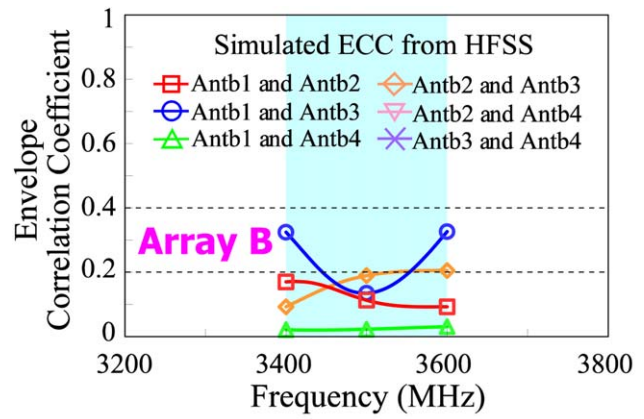
Note that the QAL arrays in Array A and B are all with same dimensions as shown in Figure 1(c). The QAL array comprises four printed open-slot antennas [14,15] configured into a linear array of compact size  $3 \times 50 \text{ mm}^2$  ( $0.035\lambda \times 0.58\lambda$ ,  $\lambda$  the wavelength at 3.5 GHz). Take the QAL array formed by Anta1, Anta2, Anta3, and Anta4 in Array A as an example, it is disposed along the upper half portion of the right side edge of the system circuit board, with a spacing of 15 mm to the top right corner. Anta1 to Anta4 are with the same size of  $3 \times 8 \text{ mm}^2$ , and their corresponding dimensions are all the same. Three neutralization lines are applied in each QAL array to achieve acceptable isolation between the antennas therein. Through proper tuning of the width and length of the neutralization lines [16,17], acceptable isolation of better than 10 dB for frequencies in the 3400–3600 MHz band is obtained. The two QAL arrays in Array B also have the same dimensions as given in Figure 1(c), and both QAL arrays are spaced by 20 mm. Array A and B are fabricated and tested. Their results are presented in the following subsection.

### 2.2. Scattering Parameters and Antenna Efficiencies of the Antennas in Array A and B

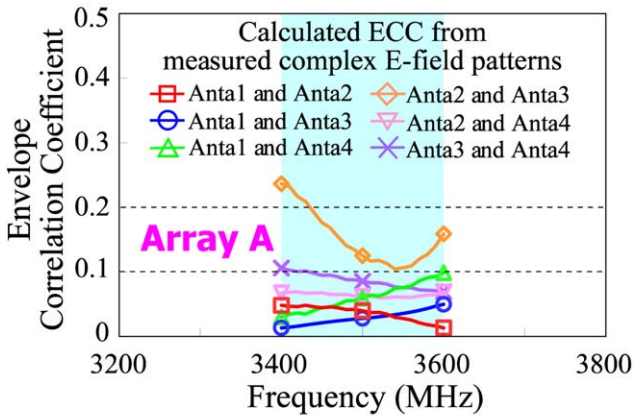
Figure 3 shows the scattering ( $S$ ) parameters and antenna efficiencies for four representative antennas (Anta1 to Anta4) in Array A. The simulated results are obtained using the full-wave electromagnetic field simulator HFSS version 15 [13]. Note that when Anta1 is excited, the remaining antennas (Anta2 to Anta8) are terminated to 50- $\Omega$  load. So is the case when Anta2 or



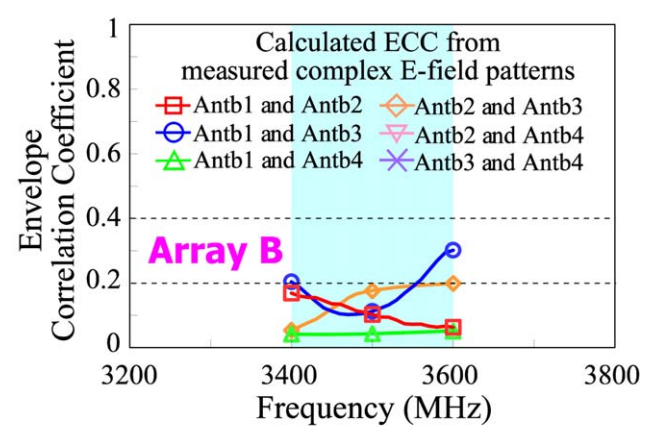
(a)



(a)



(b)



(b)

**Figure 5** (a) Simulated ECC from the HFSS and (b) calculated ECC from the measured complex electric-field patterns for the representative antennas in Array A. [Color figure can be viewed in the online issue, which is available at [wileyonlinelibrary.com](http://wileyonlinelibrary.com)]

**Figure 6** (a) Simulated ECC from the HFSS and (b) calculated ECC from the measured complex electric-field patterns for the representative antennas in Array B. [Color figure can be viewed in the online issue, which is available at [wileyonlinelibrary.com](http://wileyonlinelibrary.com)]

Anta3 or Anta4 is excited. Agreement between the simulated results and the measured data shown in Figures 3(a) and 3(b) is observed. In Figure 3(a), the measured impedance matching ( $S_{ii}$ ,  $i = 1$  to 4) of all antennas is seen to be better than about  $-6$  dB (3:1 VSWR) for frequencies in the 3400–3600 MHz band (see the colored frequency region in the figure). Good isolation of better than 10 dB for two antennas in the array in the operating band is also obtained. In Figure 3(b), it is seen that the measured antenna efficiencies which include the mismatching losses reach about 40–60% in the operating band is obtained. Also note that the results of Anta5 to Anta8 are generally the same as those of Anta1 to Anta4, owing to the symmetry of the two QAL arrays with respect to the central line of the system circuit board. The results of Anta5 to Anta8 are hence not shown for brevity.

For Array B, the  $S$  parameters and antenna efficiencies for four representative antennas (Antb1 to Antb4) therein are shown in Figure 4. Agreement between the simulation and measurement is also seen. The impedance matching ( $S_{ii}$ ,  $i = 1$  to 4) for Antb1 to Antb4 is also better than  $-6$  dB for frequencies in the 3400–3600 MHz band. The isolation is also seen to be better than 10 dB in the operating band. The antenna efficiencies, however, are about 30–52% for Antb1 to Antb4. It is noted that the antenna efficiencies of the antennas in Array B are lower than those of the antennas in Array A by about 8–

10%. This behavior is largely because the coupling between the two QAL arrays in Array B is stronger than that in Array A, owing to the relatively smaller spacing between the two QAL arrays in Array B.

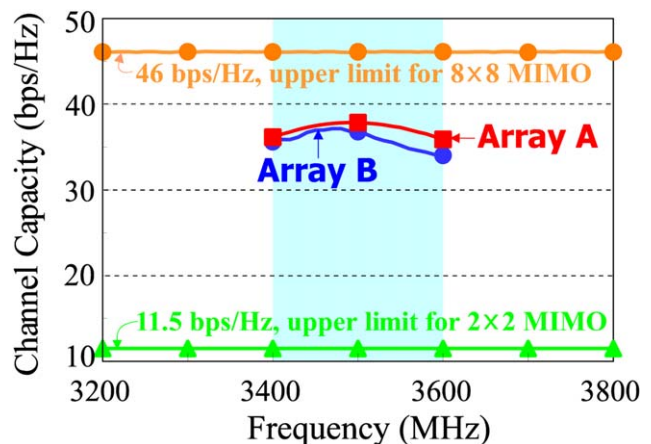


**Figure 7** Calculated channel capacities of the fabricated Array A and B in an  $8 \times 8$  MIMO system. [Color figure can be viewed in the online issue, which is available at [wileyonlinelibrary.com](http://wileyonlinelibrary.com)]

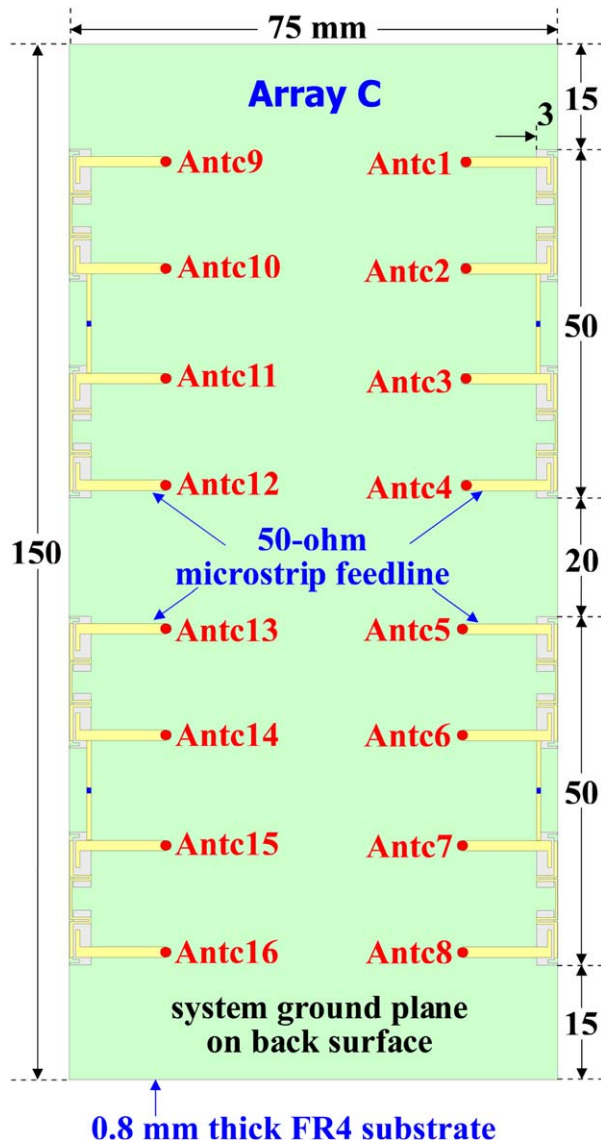
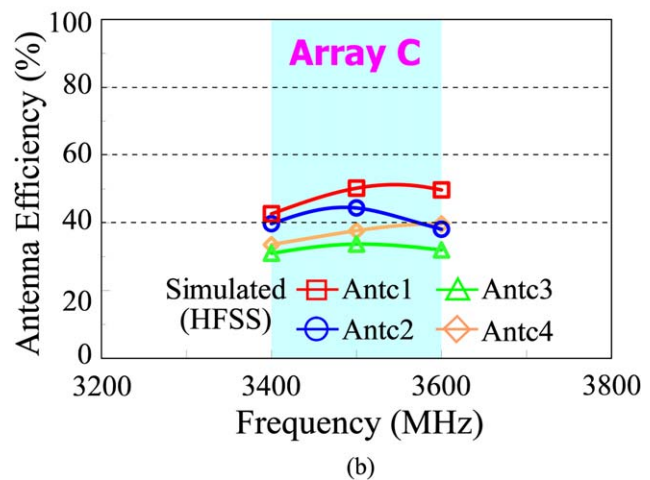
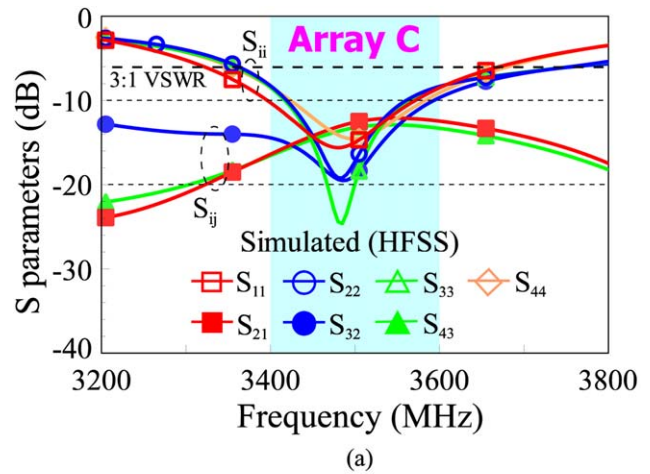


**Figure 8** Geometry of the 16-antenna array formed by four QAL arrays (Array C). [Color figure can be viewed in the online issue, which is available at [wileyonlinelibrary.com](http://wileyonlinelibrary.com)]

### 2.3. MIMO Channel Capacity

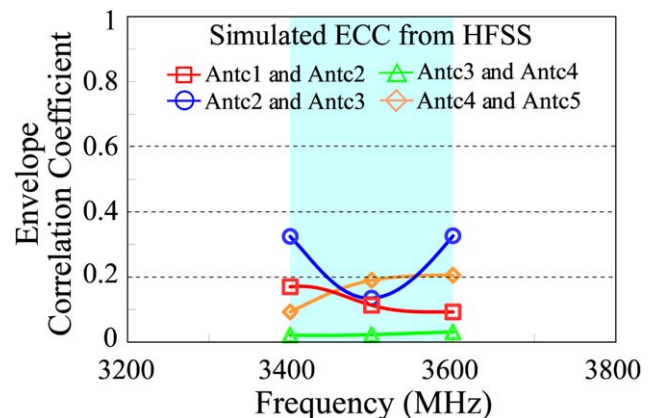
To calculate the channel capacity of Array A and B for operation in an  $8 \times 8$  MIMO system, the ECC values for the antennas thereof are studied. Figure 5 shows both values of the simulated ECC from the HFSS [13] and the calculated ECC from the measured complex electric-field patterns for the antennas in Array A. The corresponding ECC values for the antennas in Array B are shown in Figure 6. Again, only the results for Anta1 to Anta4 in Array A and Antb1 to Antb4 in Array B are presented. The remaining antennas in Array A and B are expected to have the same results as shown in Figures 5 and 6 owing to the symmetry of the two QAL arrays in Array A and B. Similar simulated and calculated ECC values are seen. For Array A and B, the ECC values in the 3.5-GHz band are less than 0.25 and 0.32, respectively. The ECC values are all less than 0.5, which makes Array A and B promising for the MIMO operation [4,6].

Figure 7 shows the calculated ergodic channel capacities of the fabricated Array A and B in an  $8 \times 8$  MIMO system. It is assumed



**Figure 9** Simulated (a)  $S$  parameters and (b) antenna efficiencies for four representative antennas (Antc1 to Antc4) in Array 3. [Color figure can be viewed in the online issue, which is available at [wileyonlinelibrary.com](http://wileyonlinelibrary.com)]

that the 8 transmitting antennas are uncorrelated with perfect antenna efficiency (100%) and the wave propagation channels are independently and identically distributed with Rayleigh fading environment [6]. The 8 antennas in Array A and B act as receiving



**Figure 10** Simulated ECC from the HFSS for the antennas in Array C. [Color figure can be viewed in the online issue, which is available at [wileyonlinelibrary.com](http://wileyonlinelibrary.com)]

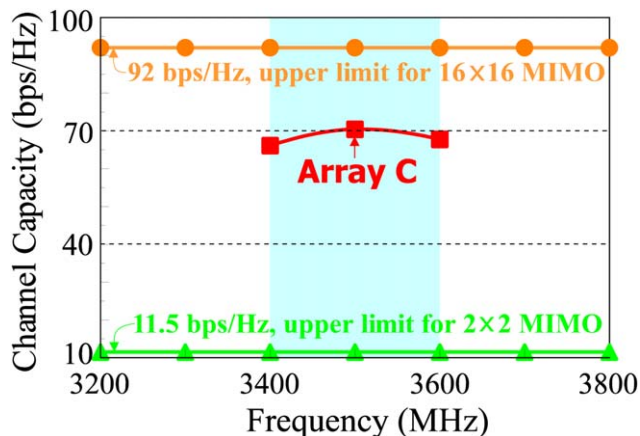


**Figure 11** Calculated channel capacities of Array C in a  $16 \times 16$  MIMO system. [Color figure can be viewed in the online issue, which is available at [wileyonlinelibrary.com](http://wileyonlinelibrary.com)]

antennas with the performances given in Figures 3–6. The results shown in the figure are obtained by averaging 10,000 Rayleigh fading realizations with a 20-dB SNR. The obtained channel capacities are about 36–38 bps/Hz for Array A and about 34–37 bps/Hz for Array B. Array A can achieve a larger channel capacity than Array B. This is reasonable, as the antennas in Array A have better antenna efficiencies and ECC values than those in Array B. It is also noted that for Array A, the maximum channel capacity reaches about 3.3 times that (11.5 bps/Hz) of the upper limit of an ideal  $2 \times 2$  MIMO system with 100% antenna efficiency for the transmitting and receiving antennas therein [6].

### 3. 16-ANTENNA ARRAY

#### 3.1. Array Configuration and Performance of the Antennas Therein

The 16-antenna array formed using four QAL arrays is also studied. Figure 8 shows the geometry of the 16-antenna array denoted as Array C in the study. The 16-antenna array can also be considered to comprise two 8-antenna arrays such as Array A or Array B. As shown in the figure, there are 8 antennas (Antc1 to Antc8 and Antc9 to Antc16) disposed along the two side edges of the system circuit board. The antenna dimensions are the same as those given in Figure 1. The simulated  $S$  parameters and antenna efficiencies for four representative antennas (Antc1 to Antc4) in Array C are presented in Figure 9. The results of Antc1 are obtained with other antennas (Antc2 to Antc16) terminated to 50- $\Omega$  loads. The results of Antc2 to Antc4 are obtained with the same testing condition. Also, from the symmetry of the array structure, it is expected that Antc8, Antc9, and Antc16 will have the same performance as that of Antc1. Similarly, Antc7, Antc10, and Antc15 will behave the same as Antc2. The results of Antc6, Antc11, and Antc14 will also be the same as that of Antc3. Those of Antc5, Antc12, and Antc13 will also be the same as that of Antc4. The results of Antc5 to Antc16 are hence not shown for brevity.

From the results shown in Figure 9(a), it indicates that the antennas in Array C can have acceptable impedance matching of less than  $-6$  dB (3:1 VSWR) in the 3400–3600 MHz band. The isolation between two antennas in Array C is still better than 10 dB. The antenna efficiencies are seen to be about 30–52% in the operating band, as shown in Figure 9(b). The performances of the antennas in Array C are seen to be similar as those of the antennas in Array B and slightly degraded as compared with those of the antennas in Array A.

#### 3.2. MIMO Channel Capacity

The simulated ECC from the HFSS for the antennas in Array C is presented in Figure 10. The ECC values for representative antennas in Array C are shown. The ECC values for the antennas in Array C are obtained to be less than about 0.32, also similar to the results of Array B and slightly larger than the results of Array A. The calculated ergodic channel capacities of Array C in a  $16 \times 16$  MIMO system with a 20-dB SNR are presented in Figure 11. In the calculation, the 16 transmitting antennas are assumed to be uncorrelated with perfect antenna efficiency (100%). The wave propagation channels are also assumed to be independently and identically distributed with Rayleigh fading environment [6]. The 16 antennas in Array C are receiving antennas with performances given in Figures 9 and 10. Results show that the channel capacities are about 66–70 bps/Hz in the 3400–3600 MHz band, which is better than about 1.8 times that (36–38 bps/Hz) of Array A and better than about 1.9 times that (34–37 bps/Hz) of Array B. When compared with the operation in an ideal  $2 \times 2$  MIMO system with 100% antenna efficiency for the transmitting and receiving antennas therein, the obtained channel capacity of Array C in a  $16 \times 16$  MIMO system is about 5.7–6.1 times the upper limit (11.5 bps/Hz) of the ideal  $2 \times 2$  MIMO system [6].

### 4. CONCLUSION

Two 8-antenna arrays and one 16-antenna array operated in the 3.5-GHz LTE band and disposed in the smartphone for the MIMO operation have been demonstrated. The 8-antenna and 16-antenna arrays are formed using the QAL array as a building block and are disposed along the narrow region between the display panel and the two long side edges of the smartphone casing. Acceptable ECC values of the antennas in these three arrays have been obtained. The minimum calculated ergodic channel capacities with a 20-dB SNR operated in the 3.5-GHz LTE band is about 36 bps/Hz for the 8-antenna array disposed along two opposite side edges, while that for the 16-antenna array can even reach about 66 bps/Hz. With a channel capacity of 66 bps/Hz and a bandwidth of 200 MHz (3400–3600 MHz), the data transmission rate can be as large as 13.2 Gbps. The proposed arrays indicate that it is promising to dispose as many as 16 antennas for the 3.5-GHz LTE MIMO operation in the limited space in the smartphone.

### REFERENCES

- H. Li, Z.T. Miers, and B.K. Lau, Design of orthogonal MIMO handset antennas based on characteristic mode manipulation at frequency bands below 1 GHz, *IEEE Trans Antennas Propag* 62 (2014), 2756–2766.
- K.L. Wong, T.W. Kang, and M.F. Tu, Internal mobile phone antenna array for LTE/WWAN and LTE MIMO operations, *Microwave Opt Technol Lett* 53 (2011), 1569–1573.
- K.L. Wong, H.J. Jiang, and T.W. Weng, Small-size planar LTE/WWAN antenna and antenna array formed by the same for tablet computer application, *Microwave Opt Technol Lett* 55 (2013), 1928–1934.
- Y.L. Ban, Z.X. Chen, Z. Chen, K. Kang, and J.L.W. Li, Decoupled closely spaced heptaband antennas for WWAN/LTE smartphone applications, *IEEE Antennas Wireless Propag Lett* 13 (2014), 31–34.
- K.L. Wong, P.W. Lin, and H.J. Hsu, Decoupled WWAN/LTE antennas with an isolation ring strip embedded there between for smartphone application, *Microwave Opt Technol Lett* 55 (2013), 1470–1476.
- K.L. Wong and J.Y. Lu, 3.6-GHz 10-antenna array for MIMO operation in the smartphone, *Microwave Opt Technol Lett* 57 (2015), 1699–1704.
- Y.S. Cho, J. Kim, W.Y. Yang, and C.G. Kang, *MIMO-OFDM wireless communications with MATLAB*, Wiley, New York, 2010.
- LTE Frequency Bands & Spectrum Allocations—a summary and tables of the LTE frequency band spectrum allocations for 3G & 4G LTE - TDD and FDD, Available at: <http://www.radio-electronics.com/>.

9. K.L. Wong and Z.G. Liao, Passive reconfigurable triple-wideband antenna for LTE tablet computer, *IEEE Trans Antennas Propag* 63 (2015), 901–908.
10. K.L. Wong and T.W. Weng, Small-size triple-wideband LTE/WWAN tablet device antenna, *IEEE Antennas Wireless Propag Lett* 12 (2013), 1516–1519.
11. A.A. Al-Hadi, J. Ilvonen, R. Valkonen, and V. Viikari, Eight-element antenna array for diversity and MIMO mobile terminal in LTE 3500 MHz band, *Microwave Opt Technol Lett* 56 (2014), 1323–1327.
12. Y.L. Ban, S. Yang, Z. Chen, K. Kang, and J.L.W. Li, Decoupled planar WWAN antennas with T-shaped protruded ground for smartphone applications, *IEEE Antennas Wireless Propag Lett* 13 (2014), 483–486.
13. ANSYS HFSS, Ansoft Corp., Pittsburgh, PA, Available at: <http://www.ansys.com/products/hf/hfss/>.
14. K.L. Wong, P.W. Lin, and C.H. Chang, Simple printed monopole slot antenna for penta-band WWAN operation in the mobile handset, *Microwave Opt Technol Lett* 53 (2011), 1399–1404.
15. C.I. Lin and K.L. Wong, Printed monopole slot antenna for internal multiband mobile phone antenna, *IEEE Trans Antennas Propag* 55 (2007), 3690–3697.
16. Y. Wang and Z. Du, A wideband printed dual-antenna with three neutralization lines for mobile terminals, *IEEE Trans Antennas Propag* 62 (2014), 1495–1500.
17. S.W. Su, C.T. Lee, and F.S. Chang, Printed MIMO-antenna system using neutralization-line technique for wireless USB dongle applications, *IEEE Trans Antennas Propag* 60 (2012), 456–463.

© 2016 Wiley Periodicals, Inc.

## AN ULTRAWIDEBAND INVERTED DOUBLE DISCONE ANTENNA WITH 150:1 IMPEDANCE BANDWIDTH

Irfan Shahid,<sup>1</sup> Fawad Hussain,<sup>1</sup> Jehanzeb Burki,<sup>2</sup> and M. Shoaib Arif<sup>1</sup>

<sup>1</sup> College of Aeronautical Engineering, NUST, Risalpur, Khyber Pakhtunkhwa, Pakistan; Corresponding author: [irfan.shahid@cae.nust.edu.pk](mailto:irfan.shahid@cae.nust.edu.pk)

<sup>2</sup> Institute of Avionics and Aeronautics, Air University E-9, Islamabad, Pakistan

Received 22 May 2015

**ABSTRACT:** In this article, an improved design of ultrawideband (UWB) inverted double disccone (IDD) antenna is presented. Conventionally, IDD antennas are designed using tapered cylindrical wires as antenna elements. The tapering makes these antennas very fragile and the antennas suffer frequent damage during installation, transportation or even, due to perching of birds during normal operation. In this work, curved metal sheets are used instead of tapered wires to improve antenna robustness with no compromise on antenna's performance. Using this approach, an IDD antenna with an ultrawide impedance bandwidth is designed, fabricated, and tested. The measurements show good conformance with design and the measured antenna demonstrates an impedance bandwidth (for  $V_{SWR} < 2$ ) of 150:1 in frequency range of 120 MHz–18 GHz with omnidirectional radiation characteristics. © 2016 Wiley Periodicals, Inc. *Microwave Opt Technol Lett* 58:181–184, 2016; View this article online at [wileyonlinelibrary.com](http://wileyonlinelibrary.com). DOI 10.1002/mop.29530

**Key words:** ultrawideband antenna; omnidirectional antenna; inverted double disccone antenna; impedance bandwidth

### 1. INTRODUCTION

Disccone antennas are commonly used for wideband applications and exhibit a dipole like radiation pattern. These structures provide a nominal impedance bandwidth of 8:1 and pattern bandwidth of approximately 5:1 [1]. A variety of modifications in disccone antennas have been proposed for ultrawideband (UWB)

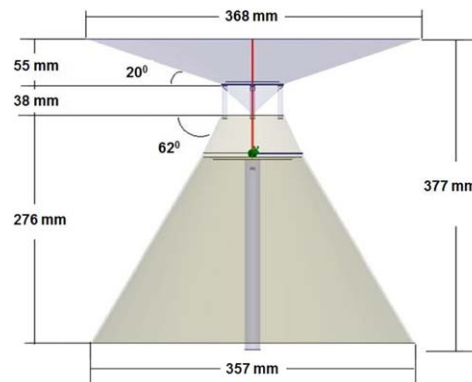


**Figure 1** Side view model of the proposed ultrawideband IDD antenna for 120 MHz–18 GHz omnidirectional applications. [Color figure can be viewed in the online issue, which is available at [wileyonlinelibrary.com](http://wileyonlinelibrary.com)]

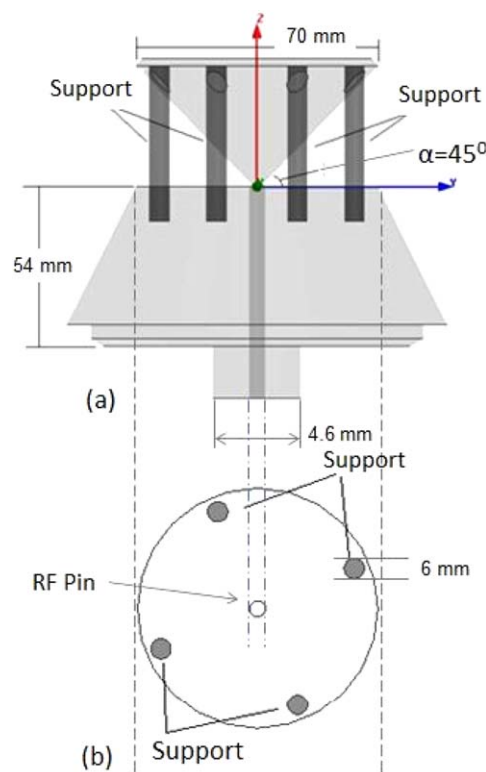


**Figure 2** Detailed model of the connection assembly joining the two inverted disccones. (a) Side view of complete assembly (b) top view of the lower disccone assembly showing holes for upper disccone supports and RF feed. [Color figure can be viewed in the online issue, which is available at [wileyonlinelibrary.com](http://wileyonlinelibrary.com)]

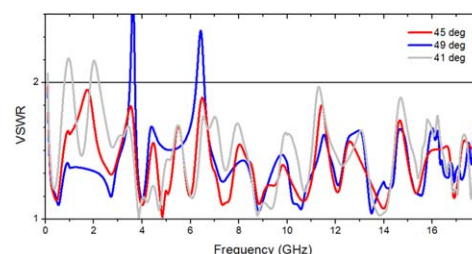


**Figure 3** Simulated results showing the effect of disccone assembly taper angle  $\alpha$  on antenna's impedance bandwidth for  $V_{SWR} \leq 2$ . [Color figure can be viewed in the online issue, which is available at [wileyonlinelibrary.com](http://wileyonlinelibrary.com)]